Shock Waves (2005) 14(4): 251–258
DOI 10.1007/s00193-005-0269-2

ORIGINAL ARTICLE

A. Bourgoing · Ph. Reijasse

Experimental analysis of unsteady separated flows in a supersonic planar nozzle

Received: 21 February 2004 / Accepted: 20 June 2004 / Published online: 25 October 2005

Abstract The unsteady aspects of shock-induced-separation patterns have been investigated inside a Mach 2 planar nozzle. The mean location of the shock can vary by changing, relatively to the nozzle throat, the height of the second throat which is positioned downstream of the square test section. This study focuses on the wall pressure fluctuations spectra and the unsteady behaviour of the shock. Symmetric shock configurations appear both for the largest openings of the second throat, and for the smallest openings. For an intermediate opening the shock system exhibits asymmetrical configurations. A coating with roughnesses sticked on the throat part of the nozzle in order to modify the state of the incoming boundary layers (from smooth to rought turbulent statement) is a driver for the asymmetry. The fluctuating displacements of the shock patterns were analysed by using an ultra fast shadowgraph visualization technique. A spectral analysis of the unsteady wall pressure measurements has revealed low frequency phenomena governed by large structure dynamics in the separated flows.

Keywords Supersonic separated flow · Asymmetrical shock · Fluctuating pressure · Wall roughness

PACS 02.60.Cb; 05.10.Ln; 47.11.+j; 47.15.Cb; 47.40.Nm

1 Introduction

Flow separation inside propulsive nozzles generates unsteady and asymmetrical shock structures and induce fluctuating side loads which can damage the structure. Fundamental experiments investigated the flow separation occurring in various types of nozzle [1–4]. Even if some explanations of fluctuating pressure loads behaviour were proposed in compression ramp flow fields [5, 6], their origin is not well known. And the lack of information on the basic aerodynamic behaviour of separated flows in nozzle still remains.

Salmon et al. [7] and Sajben et al. [8] showed experimentally by one-dimensional Laser Doppler velocimetry, the behaviour of an unsteady detached flow produced by a boundary layer–shock interaction in a transonic planar diffusor nozzle. These studies have well characterised the nature of the recirculated flow constituted by a maximum velocity of about 25% of the external velocity U and the fluctuations of the longitudinal velocity component $\sqrt{u'^2}$ of about 50% of U.

Experimental studies in transonic regime at an upstream Mach number of 1.4 permitted to characterize precisely the shock structure induced by a two-dimensional nozzle [9]. The longitudinal velocity and the turbulent kinetic energy profiles in the detached flow are similar to an isobaric turbulent jet mixing layer theoretical solution obtained by Görtler [10].

The fluctuating and asymmetrical aspects of flow separation inside nozzles were shown and described by Lawrence [2]. The author performed experimental studies by modifying the pressure ratio and the divergence angle in planar and axisymmetric nozzles with cold gas and underlined some stable and unstable configurations. Thompson [11], studied the nature of flow asymmetry by regarding its sensitivity to downstream flow conditions.

The purpose of this article is to present a detailed description of the fluctuating aspects of shock-induced separated flows in a two-dimensional planar nozzle with symmetric and asymmetric shock structure configurations [12]. A rapid flow visualization technique and pressure measurements have permitted to underline the fluctuations of characteristic points of the symmetric and asymmetric shock patterns. In addition, the influence of the incoming boundary layer state on the asymmetry of the shock pattern was studied.

Communicated by K. Takayama

A. Bourgoing · P. Reijasse (✉)
Fundamental and Experimental Aerodynamics Department
Office National d'Etudes et de Recherches Aérospatiales
92190 Meudon France
E-mail: Philippe.Reijasse@onera.fr

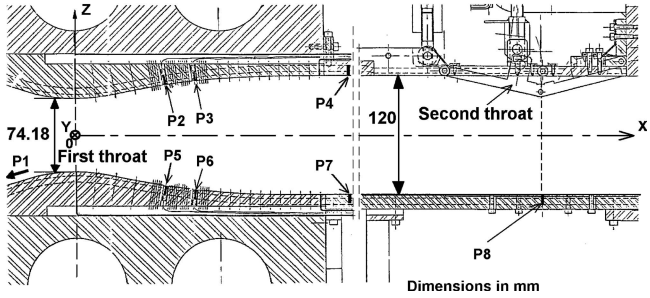

Fig. 1 Schematic of the S8Ch wind tunnel

2 Apparatus and experimental set-up

2.1 Wind tunnel

The experimental set-up is constituted by two planar half-nozzles producing a uniform Mach number of 1.95 in the exit plane. The wind tunnel is fed with desiccated air having the following stagnation conditions: pressure $p_{i0} = 98{,}000 \pm 800$ Pa, temperature $T_{i0} = 305 \pm 10$ K. The square test section is 120 mm $\times$ 120 mm. The unit Reynolds number based on the exit velocity $U_e = 514\ \mathrm{m\,s^{-1}}$ is about $1.2 \times 10^7\ \mathrm{m^{-1}}$. The partial unstarting of the planar nozzle is initiated by the mean of a variable throat placed downstream of the test section.

Different shock configurations are obtained by changing the second-to-primary throat contraction ratio $\tau = h_2/h_1$, where h_1 and h_2 are, respectively, the first and second throat heights. The schematic of the wind tunnel is presented in Fig. 1.

2.2 Optical system

An optical system based on the Cranz–Schardin visualization technique has been developed at Onera [13] in order to perform ultra fast shadowgraphs of unsteady flow with high pressure gradients.

The apparatus is constituted by an emitting and a collecting part represented in Fig. 2. The emitting part consists in a device able to produce a train of 24 sparks with a lag time of 400 μs controlled by an electronic trigger. The duration of each spark is about 300 ns. Each spark is transformed into a parallel beam by a first spherical mirror. This beam is deviated by a plane mirror and crosses the test set-up. The collecting part records a sequence of 24 instantaneous shadowgraphs. In this configuration, the shadowgraph system integrates the second derivative of the density gradient along the flow span. The visualised field has a diameter of 250 mm.

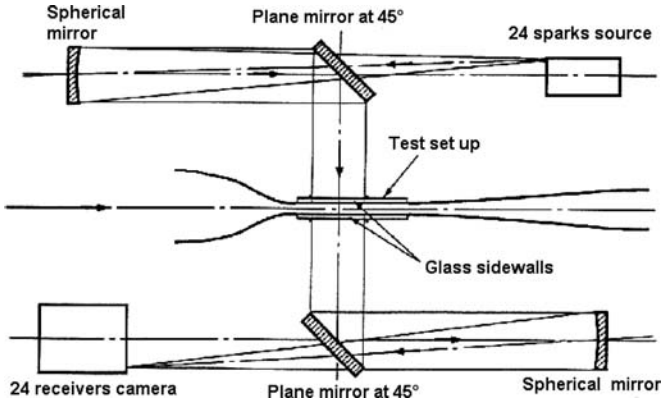

Fig. 2 Schematic of the ultra fast shadowgraph system

2.3 Wall pressure measurements

Eight fast response pressure transducers are installed on the lower and upper walls. The transducer $P1$ (5*psid*) measures the pressure in the settling chamber. The transducers $P2$–$P7$ (15*psid*) are installed in the divergent part of the nozzle in opposite position. $P8$ is located on the lower wall opposite to the second throat (see Fig. 1).

3 Results and discussion

3.1 Shock pattern behaviour

For a given contraction ratio and during the start-up transient of the nozzle, a complex shock structure moves towards the second throat area along the test section and becomes stable in the divergent part of the nozzle. The main feature of the shock system is the presence of a quasi-normal shock ended by two lambda-shock structures. Three domains of contraction ratio τ have been distinguished according to the shock pattern. For the largest openings (τ critical > 1.28) symmetrical shock configurations are obtained (see Fig. 3).

For the contraction ratio τ critical $= 1.28$, the shock patterns are generally asymmetrical. Two possible asymmetrical shock structures with the largest lambda structure either located on the lower wall or on the upper wall could occur (see Fig. 4a–b). Once permanent flow regime is established in the test section for τ critical $= 1.28$, the obtained asymmetrical pattern is stable. The flow asymmetry is determined during the start-up transient. Further testings have verified that the asymmetrical geometry of the second throat was not the driver of the shock asymmetry. Still, for the critical value τ critical $= 1.28$, a symmetrical pattern was sometimes observed (Fig. 4c).

This symmetrical pattern is much less stable than the previous asymmetrical ones. The existence of symmetrical and asymmetrical structures must be attributed to the conjunction of slight variations of flow stagnation conditions during a test [12], with pressure fluctuations inside separated zones. For the smallest contraction ratios ($\tau < 1.24$), the shock pattern keeps a symmetrical aspect but this symmetry is not as good as for $\tau = 1.36$ and $\tau = 1.35$ (see Fig 5).

Schematic interpretations in a two-dimensional representation of shock pattern are presented in Fig. 6. The shock/boundary layer interaction produces two separated

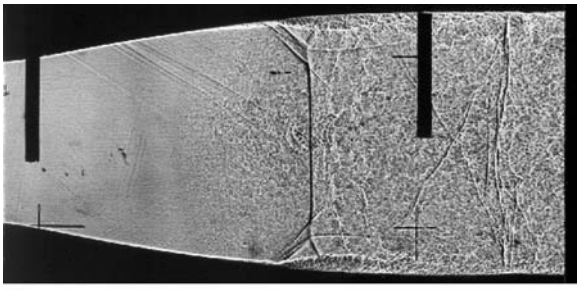

a) $\tau = 1.36$

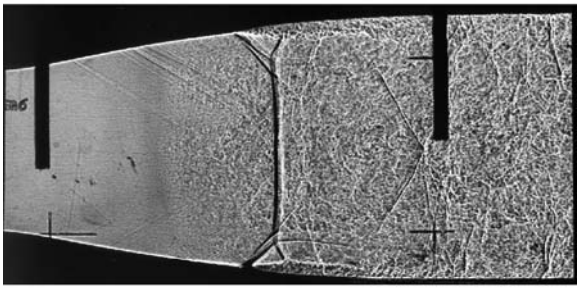

b) $\tau = 1.35$

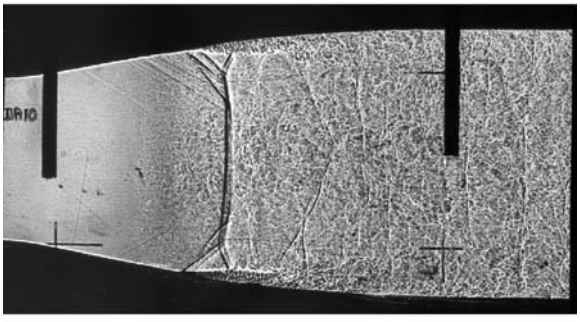

c) $\tau = 1.31$

Fig. 3 Symmetrical shock patterns for $\tau > \tau$ critical

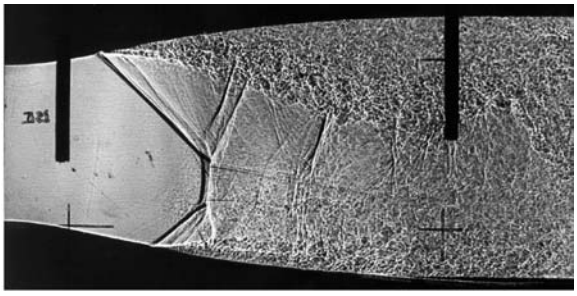

a) τ *critical* $= 1.28$ *asymmetric type 1*

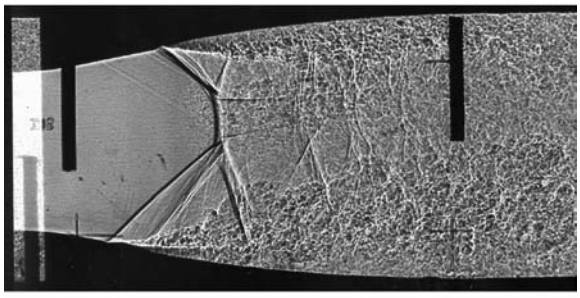

b) τ *critical* $= 1.28$ *asymmetric type 2*

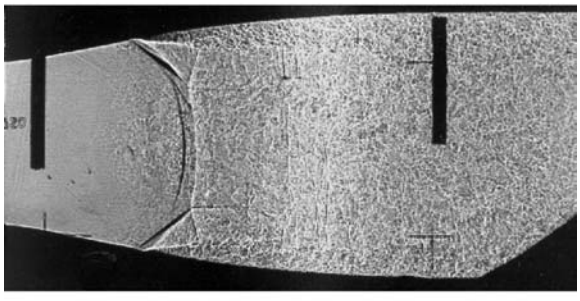

c) τ *critical* $= 1.28$ *symmetric*

Fig. 4 Symmetrical and asymmetrical shock patterns for τ critical $=$ 1.28

flows with reattachment downstream. The interaction between the two oblique shocks $(C1)$ and $(C3)$ forms a Mach disk $(N1)$ slightly curved here. This interaction is of type 2 according to Edney [14] classification. The lambda-shock structures $(C1) - (C2)$ and $(C3) - (C4)$ are jointed to $N1$ by two triple points $T1$ and $T2$.

The difference in velocity between the flows downstream $(C2)$ and $(C4)$ and the quasi-normal shock $(N1)$ produces two slip lines $L1$ and $L2$ coming from $T1$ and $T2$. These slip lines form a fluidic boundary like convergent nozzle producing a flow re-acceleration until a supersonic regime. The interactions of $(C2)$ and $(C4)$ on the detached mixing layers produce reflection waves which reflect on slip lines and form secondary shocks $(C2')$ and $(C4')$. Trailing oblique shocks are thus confined between the slip line and the detached mixing layers until the flow reach subsonic conditions.

In Fig. 6b, the upper lambda-shock structure is clearly greater the lower one. Consequently, separation and detachment points are shifted compared to the symmetrical case. Due to this strong asymmetry, the upper mixing layer is deviated towards the bottom preventing the lower

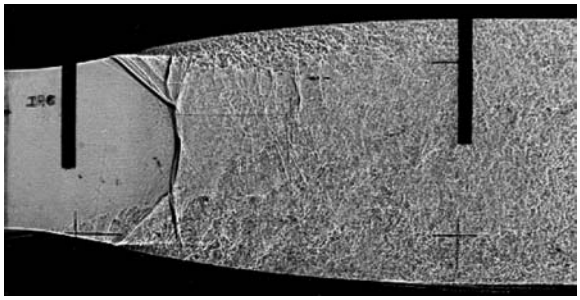

Fig. 5 Symmetrical shock pattern for $\tau < \tau$ critical

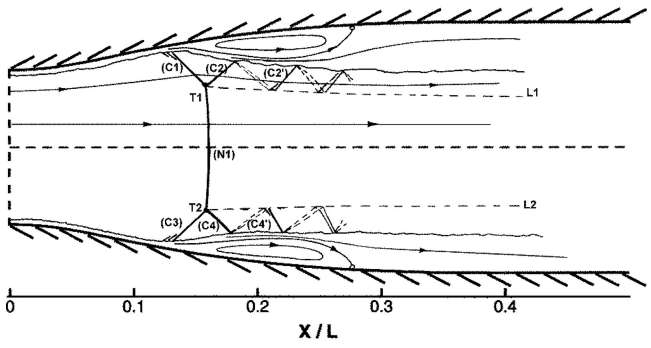

a) τ *critical* $= 1.28$ *symmetric*

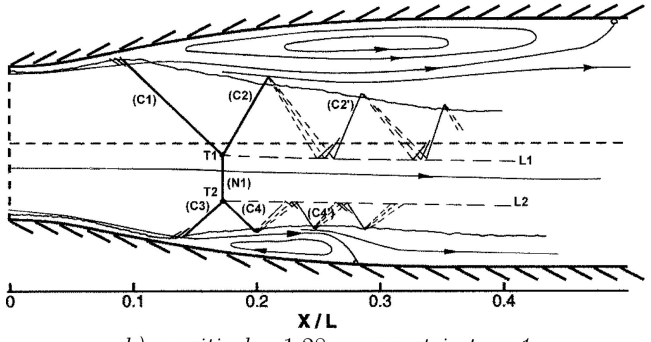

b) τ *critical* $= 1.28$ *asymmetric type 1*

Fig. 6 Symmetrical and asymmetrical shock patterns for τ critical $=$ 1.28

recirculation expansion. We find again after $(C2)$ and $(C4)$ trailing shock and expansion waves as in the symmetrical case.

3.2 Shock pattern displacements

A quantitative analysis of shock movements has been performed from rapid sequences of 24 spark shadowgraphs. The positions of some characteristic points of the shock structures were recorded. Longitudinal and vertical displacements of the two triple points $T1$ and $T2$, the feet of the upstream oblique shocks $D1$ and $D2$ and the ends $A1$ and $A2$ of the downstream legs of the lambda-shock structures $(C2)$ and $(C4)$ have been noted (Fig 7).

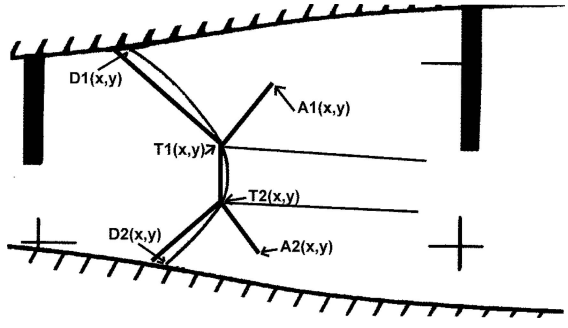

Fig. 7 Characteristic points of the shock structure

The longitudinal displacements for the configuration $\tau = 1.36$ reveal a motion of all the characteristical points in phase which seem to fluctuate at a frequency of 300 Hz. A large amplitude (see Fig. 8) of the longitudinal fluctuation is observed and can reach 10 mm. The vertical displacements are not very important (between 2 and 4 mm), thus, shock oscillations are mainly longitudinal. The longitudinal amplitudes for the configuration $\tau = 1.35$ are about 4 mm, less than in the previous case (see Fig. 9). The shock structure seems to move in phase but a lack of measurement point has not permitted to determine a dominant frequency.

From the three different configurations obtained at the contraction ratio τ critical $=$ 1.28 only the symmetrical shock and the type 1 asymmetrical shock are presented (see Figs. 10 and 11). Unlike to symmetrical configurations presented before, there is no clearly identified periodic movements. Nevertheless, we cannot exclude lower frequency shock movements. The shock movements of the symmetrical case (see Fig. 10) are non-correlated. The longitudinal and vertical displacements are in the same order of amplitude. For the type 1 asymmetrical case, the vertical displacements are important and exceed the longitudinal values especially for $T1$ and $T2$ (Fig. 11). We can explain this difference by the nature of the recirculating flows. The upper separated zone is the seat of an intense recirculation about eight times bigger in volume than on the lower wall. We can estimate the length of the recirculation region of about 70 times the upstream boundary layer thickness. It has been verified that the upper detached mixing layer includes high levels of spanwise rotational due to coherent vortical structures [15]. These structures contribute to the longitudinal and vertical shock displacements. The triple points $T1$ and $T2$ move in phase.

The configuration $\tau = 1.24$ (see Fig. 5) looks quasi-symmetrical but in fact the shock structure movements present higher longitudinal and vertical displacements which seem to be non-correlated. We can noticed there is no peculiar periodic movement of the shock (see Fig. 12). Characteristical points were difficult to localize because of important three-dimensional effects.

3.3 Transient shock pattern switch study

During the transient start up of the nozzle with no second throat the asymmetrical type 2 case naturally switches towards the symmetrical one as it has been already observed in [2] experiments. In accordance with this author, pressure fluctuations inside separated zones play an essential role in the switch phenomenon.

Four spark Schlieren visualizations were presented in Fig. 13 among a sequence recorded with a time lag of 4 ms. The first photograph, recorded with a t_0 time reference, shows a type 2 asymmetrical shock pattern. In Fig. 13b at t_0+4 ms, the separation point in the lower wall moves downstream and consequently produces a reduction of the lower

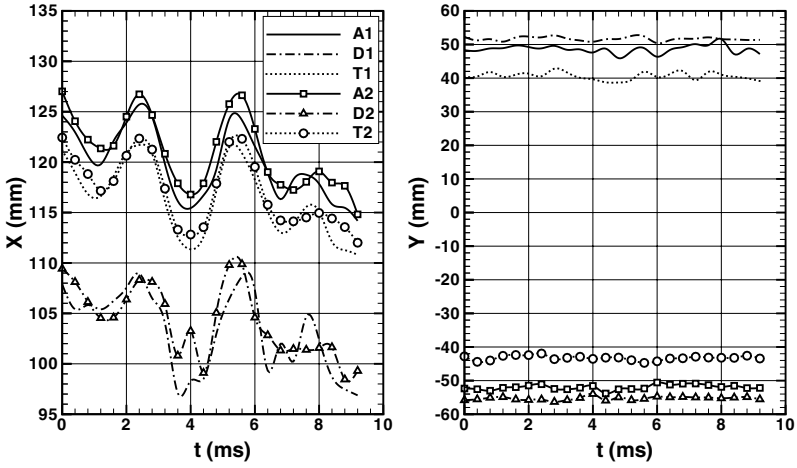

Fig. 8 Longitudinal and vertical displacements for $\tau = 1.36$

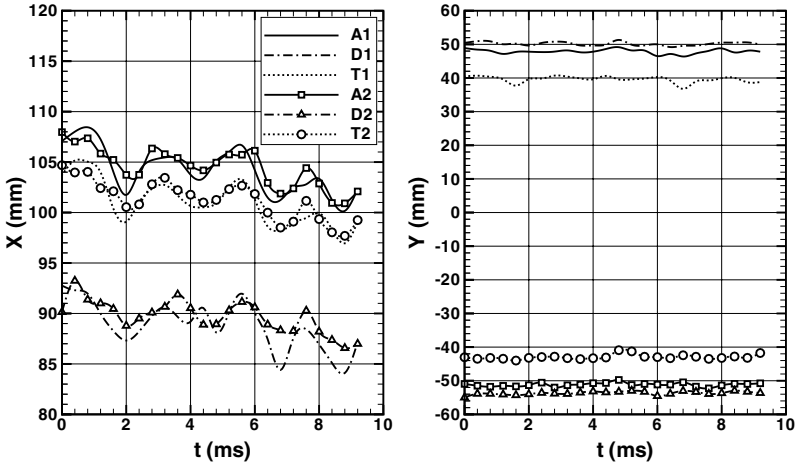

Fig. 9 Longitudinal (*left*) and vertical (*right*) displacements for $\tau = 1.35$

lambda-shock structure. At $t_0 + 8$ ms, the evolution of the separation point continues although the upper shock structure does not change any more (Fig. 13b). This motion distorts the lower lambda-shock pattern. The lower triple point T2 is pushed away to the upper triple point T1. The lower second lambda leg is almost vanished, replaced by compression waves. The normal shock and the first lambda leg merge into a kind of curve shock structure. This configuration is unstable and tends to adopt a symmetrical aspect seeing in Fig. 13d.

3.4 Wall pressure fluctuations

The wall pressure fluctuations have been measured at a 10 kHz sampling rate by fast response transducers. The power spectral density (PSD) functions of asymmetrical case type 1 presented in Fig. 14, show a large frequency band, without peculiar dominant peak, around 60 Hz for all the transducers except for $P4$ and $P7$ which are located after the reattachment areas. This frequency band is probably due to large eddy structures in the separated flow. The second frequency domain, better defined, around 250 Hz is less energetic.

We can see the same two different frequency domains for the symmetrical case in Fig. 15. Compared to the asymmetrical case, one sees a more extensive frequency domain beneath 100 Hz. In the second frequency domain, the $P5$ and $P6$ transducers located in the separated zone show a frequency peak around 310 Hz. In accordance with theatrical works on normal shock motions in channel flows which predict a frequency band between 200 and 300 Hz [16], we can say this second frequency domain is due to shock oscillation itself.

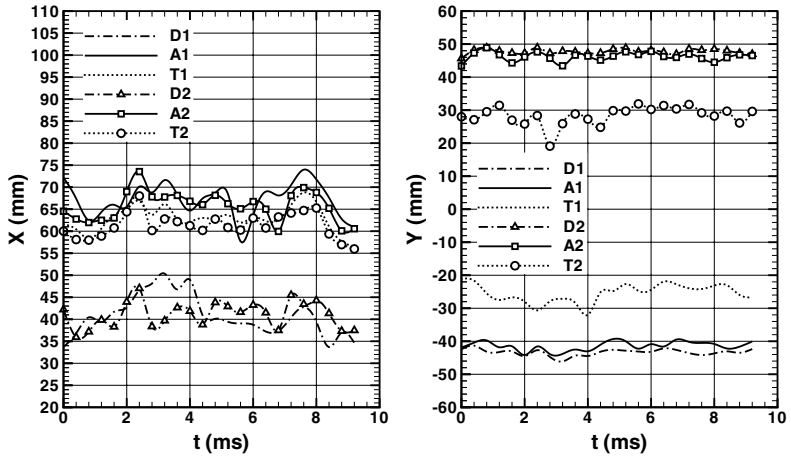

Fig. 10 Longitudinal (*left*) and vertical (*right*) displacements for τ critical $= 1.28$ – symmetrical case

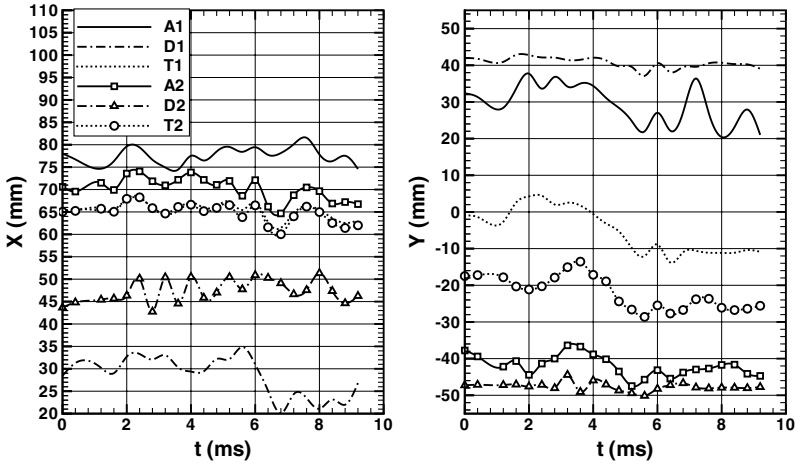

Fig. 11 Longitudinal (*left*) and vertical (*right*) displacements for τ critical $= 1.28$ – asymmetrical shock type 1

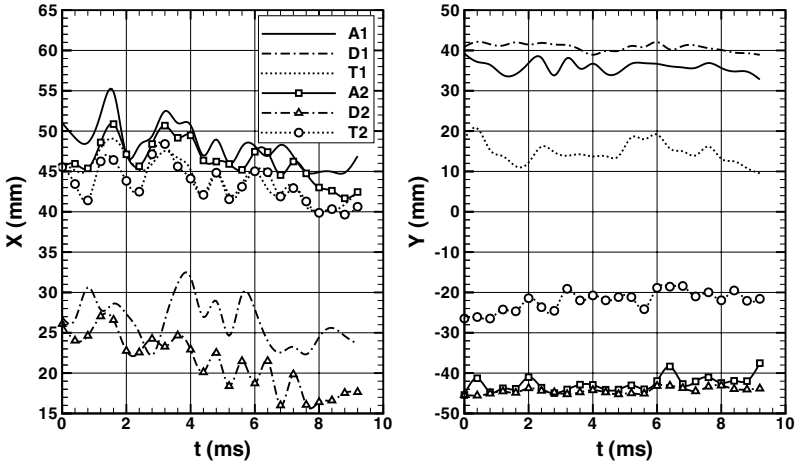

Fig. 12 Longitudinal (*left*) and vertical (*right*) displacements for the configuration $\tau = 1.24$

3.5 Wall roughness influence

In a way to study the response of separated flows to upstream boundary layer perturbations, strips of rough coating have been sticked on nozzle walls in the throat region. Coatings modify the boundary layers from smooth to rought turbulent statement in the first throat region.

When coatings are sticked on the upper and the lower walls, they produce the symmetrical shock structure. The roughnesses are assumed to be consistently distributed with a typical average height of 1 mm. The PSD functions of pressure fluctuations show peaks at a frequency around 40 Hz for all the transducers for the symmetrical case (see Fig. 16) which is quite different from the case without rough coating. In this case, the interaction between the two oblique shocks is regular and the separated zones reattach downstream of the $P4$ and $P7$ locations.

The asymmetry of the shock pattern can be forced by applying a strip of rough coating on one of the walls. Application of rough coating on the lower wall produces an asymmetrical configuration turned towards the lower wall much more pronounced than in the case without roughnesses. The main effect of the asymmetry amplification is to increase the size of the upper separated zone and to shift the reattachment point location farther downstream.

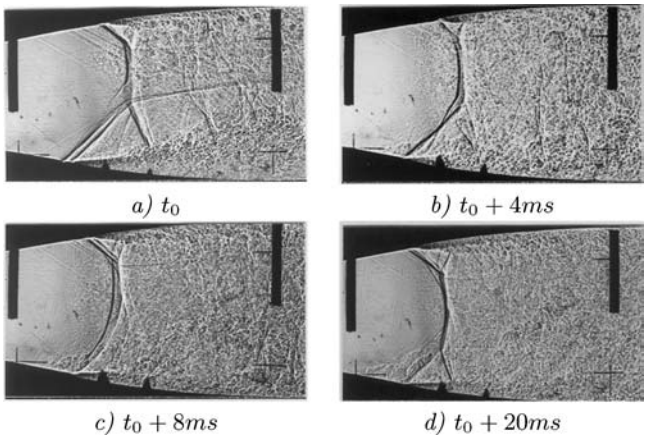

Fig. 13 Start-up transient: evolution from an asymmetrical type 2 to a symmetrical configuration

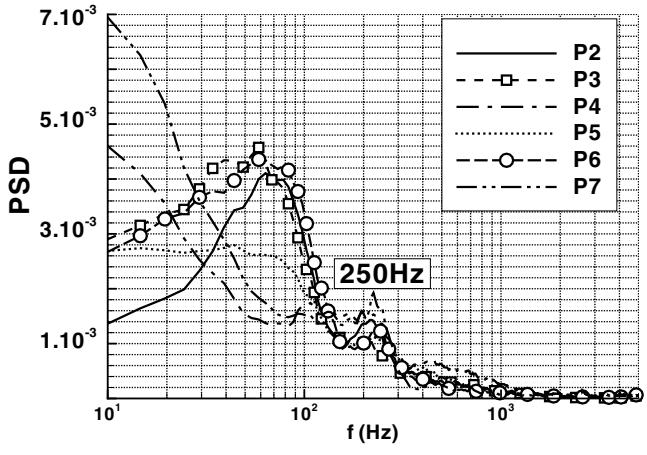

Fig. 14 PSD functions for the asymmetrical case τ critical $= 1.28$ type 1

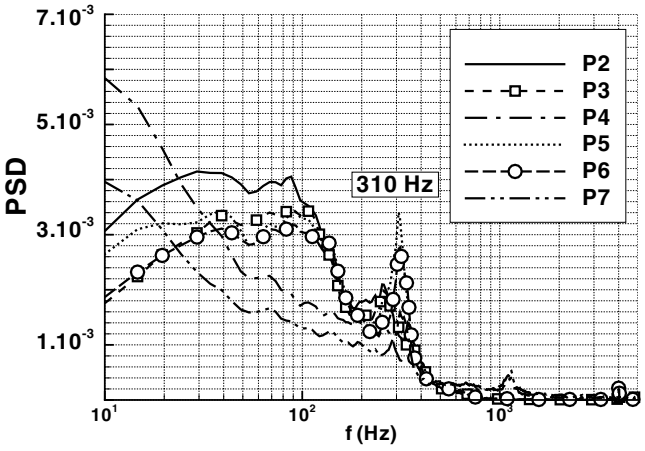

Fig. 15 PSD functions for the symmetrical case τ critical $= 1.28$

Figure 17 gives the PSD functions for the asymmetrical configurations with rough coating applied on the lower wall. As in Fig. 16, a single frequency band around 40–50 Hz is shown, instead of two frequency domains obtained, in the case without rough coating. The maximum energy level is obtained for the transducer $P4$ located far downstream of the re-attachment point.

Application of roughnesses amplifies the separation regions in all the cases and fixes the asymmetry if only one side of the divergent is modified. Since the BL velocity profile becomes less filled, the BL momentum thickness is higher, and the BL separates more precociously. Thus, the state of the incoming boundary layers has an impact on the position of the asymmetry. So, it

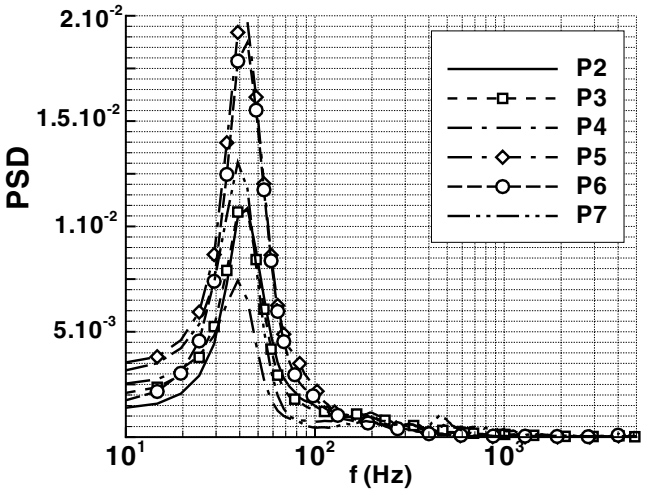

Fig. 16 PSD functions for the symmetrical case τ critical $= 1.28$ with rough coating on upper and lower walls

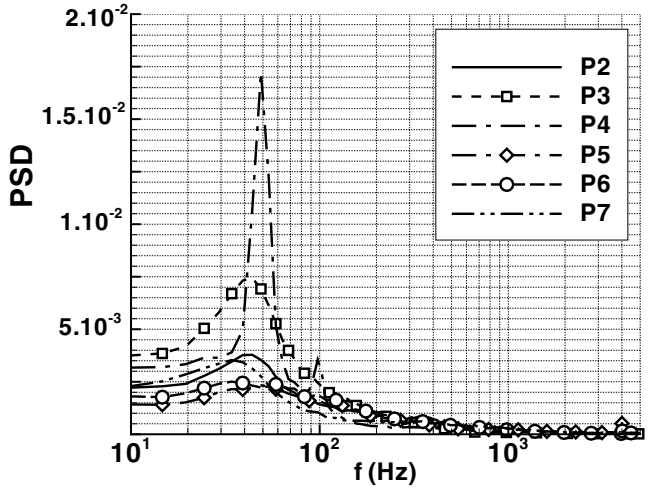

Fig. 17 PSD functions for the asymmetrical case τ critical $= 1.28$ with rough coating on lower wall

can be possible to force the asymmetry in a planar nozzle configuration but this asymmetrical aspect will bring high-level energy located in a low frequency band of 40–60 Hz.

4 Conclusions

Ultra fast shadowgraphs have provided the detailed description of the shock structure motion for several configurations obtained in an overexpanded planar nozzle. The locations of some characteristic points of the shock patterns for four different configurations were recorded. The most downstream symmetric patterns fluctuate mainly in phase in the longitudinal direction. An asymmetrical shock pattern was obtained. The points characterising the lambda-shock pattern seem to be not correlated and fluctuate both in the vertical and longitudinal directions.

In order to modify the state of the incoming boundary layers, tests were performed by application of strips of rough coating on the nozzle walls. It has been found that modification of the wall roughnesses on only one side induces the asymmetry. The shock patterns were strongly modified, the separated zones being amplified, in particular the reattachment points were shifted farther downstream. This amplification produces high wall pressure fluctuation levels, about five times more important than in the cases without roughnesses.

Acknowledgements The authors express their sincere thanks to the Space French Agency (CNES) for their support.

References

1. Green, L.: Flow separation in rocket nozzle. ARS J., pp. 34–35 (1953)
2. Lawrence, R.A.: Symmetrical and unsymmetrical separation in supersonic nozzles. Research report 67-1, Southern Methodist University (1967)
3. Carrière, P., Sirieix, M., Solignac, J.L.: Similarity properties of the laminar and turbulent separation phenomena in a non-uniform supersonic flow. In: 12th International Congress of Applied Mechanics, Springer-Verlag (1968)
4. Nave, L.H., Coffey, G.A.: Sea level side loads in high-area-ratio rocket engines. AIAA Paper 73-1284 (1973)
5. Dolling, D.S.: Fluctuating loads in shock wave/turbulent boundary layer interaction: Tutorial and update. AIAA, 93–284 (1993)
6. Erengil, M.E., Dolling, D.S.: Physical causes of separation shock unsteadiness in shock wave/turbulent boundary-layer interactions. AIAA Paper 93-3134 (1993)
7. Salmon, J.T., Bogar, T.J., Sajben, M.: Laser velocimeter measurements in unsteady separated transonic diffuser flows. AIAA Paper 81-1197 (1981)
8. Sajben, M., Bogar, T.J.: Unsteady transonic flow in a two-dimensional diffuser: interpretation of experimental results. Technical Report MDC nQ0779, Mac Donnel Douglas Corp. (1982)
9. Délery, J., Marvin, J.G.: Shock-wave boundary layer interaction. AGARDograph, AG-280 (1986)
10. Schlichting, H.: Boundary-Layer Theory. McGraw Hill (1968)
11. Thompson, R.L.: A study of the effects produced by asymmetrical nozzle entrance geometries on the downstream supersonic flow. Air Force Institute of Technology, Wright-Patterson AFB Ohio (1968)
12. Reijasse, P., Corbel, B., Soulevant, D.: Unsteadiness and asymmetry of shock-induced separation in a planar two-dimensional nozzle: a flow description. AIAA Paper 99-3694 (1999)
13. Desse, J.M., Bourez, J.P.: Visualisations ombroscopiques ultra-rapides dans la soufflerie S8 de Chalais-Meudon (Rapid shadowgraph in the S8Ch wind tunnel). ONERA report IMFL 96/66 (1996)
14. Edney, B.: Anomalous heat transfert and pressure distributions on blunt bodies at hypersonic speeds in the presence of impinging shock. FFA, Technical Report no. 115 (1968)
15. Bourgoing, A.: Instationnarité et dissymétrie d'un écoulement supersonique décollé dans une tuyère plane (*Unsteadiness and Asymmetry of a Detached Supersonic Flow in a Planar Nozzle*. PhD report. Paris 6 university (2002)
16. Robinet, J.C., Casalis, G.: Linear stability analysis in transonic diffusers flow. Aerospace Sci. Technol. **1**, 37–47 (1998)